Engineering Computations

Analysis of ice load on conical structure with discrete element method
Shunying Ji Shaocheng Di Shewen Liu

Analysis of ice load on conical structure with discrete element method

Shunying Ji and Shaocheng Di
State Key Laboratory of Structural Analysis for Industrial Equipment, Dalian University of Technology, Dalian, China, and
Shewen Liu
China Offshore Technology Center, ABS Greater China Division, Shanghai, China

Received 22 April 2014
Revised 18 July 2014
Accepted 18 July 2014

Abstract

Purpose – In oil/gas exploitations of ice-covered cold regions, conical offshore structures are designed to reduce ice force and to avoid the ice-induced intense vibrations of vertical structures. The purpose of this paper is to investigate the interaction between ice cover and conical offshore structures, the discrete element method (DEM) is introduced to determine the dynamic ice loads under different structure parameters and ice conditions.

Design/methodology/approach – The ice cover is dispersed into a series of bonded spherical elements with the parallel bonding model. The interaction between ice cover and conical offshore structure is obtained based on the DEM simulation. The influence of ice velocity on ice load is compared well with the experimental data of Hamburg Ship Model Basin. Moreover, the ice load on a conical platform in the Bohai Sea is also simulated. The ice loads on its upward and downward ice-breaking cones are compared.

Findings – The DEM can be used well to simulate the ice loads on conical structures. The influences of ice velocity, ice thickness, conical angle on ice loads can be analyzed with DEM simulations.

Originality/value – This DEM can also be applied to simulate ice loads of different offshore structures and aid in determining ice load in offshore structure designs.

Keywords Sea ice, Conical offshore structure, Discrete element method (DEM), Ice load

Paper type Research paper

1. Introduction

In ice-covered regions, the ice force is the dominant environmental factor for the structure's design. Ice loads bring more damage to the offshore structures than that of other environmental factors, such as wind and wave. When interacting with conical structures, the ice covers fail in bending mode. In contrast, when interacting with vertical structures, the ice covers fail in crushing mode. Thus, the ice-induced loads for conical structures are much lower than the loads for vertical structures (Daley *et al.*, 1998; Yue and Bi, 2000; Brown and Määttänen, 2009; Huang and Li, 2011). By reducing the peak loads, the ice-breaking cone can effectively reduce the ice-induced vibration, especially avoiding the resonant vibration of vertical jacket structures. Recently, more than ten conical structures have been established in the Bohai Sea, on which ice-reduced vibrations are significantly reduced comparing to the vertical structures. But the ice-induced vibrations of conical structures were also measured in the field

This study is financially supported by the Special Funding for National Marine Commonwealth Industry of China (Grant No. 201105016, 2012418007), the National Natural Science Foundation of China (Grant No. 41176012), and the American Bureau of Shipping (ABS).

Engineering Computations: International Journal for Computer-Aided Engineering and Software
Vol. 32 No. 4, 2015
pp. 1121-1134
© Emerald Group Publishing Limited
0264-4401
DOI 10.1108/EC-04-2014-0090

observation in the Bohai Sea (Qu *et al.*, 2006; Yue *et al.*, 2007). Therefore, it is still necessary to study the interaction between sea ice and conical structures for structure design and fatigue analysis.

During the interaction between ice cover and conical structure, the ice load is related to ice conditions (ice type, strength and velocity) and structural parameters (cone angle, cone diameter, upward or downward of cone surface, structure mass and stiffness). Different ice parameters and structural types result in various failure modes and ice loads (Dempsey, 2000). Whatever the failure mode, sea ice cover presents an obvious conversion from continuum to discontinua. Thus, the discrete element models in the last decade (Selvadurai and Sepehr, 1999; Lau *et al.*, 2011; Paavilainen and Tuhkuri, 2012) have been developed to describe the discrete characteristics of ice cover during the ice-structure interaction. If considering the pancake ice, ice ridge and rafted ice, the discrete element models have been applied more widely (Hopkins *et al.*, 2004; Sun and Shen, 2011).

In the numerical simulation of ice loads on offshore structures, the discrete element methods (DEM) have been developed using different element shapes. In the early works, the 2D disk was adopted to model ice loads of pancake ice in broken ice (Hansen and Løset, 1999a, b). Recently, the 3D polyhedral elements have been developed to simulate the ice cover. The software of 3D block DEM (DEICE3D) was adopted to simulate the interaction between ice and conical structures (Lau *et al.*, 2011). The 3D DEM with polyhedral shapes were also adopted to simulate the punch through tests of ice rubble. The simulated data compared well with the laboratory tests (Polojarvi *et al.*, 2012). Therefore, the discrete element models have been widely applied in the investigations of ice loads. Many results have been obtained to reveal the ice mechanics during the interaction between offshore structure and ice cover.

In the DEM simulations of ice loads on offshore structures, the breakage of ice cover can be obtained with bonded elements. In this study, we develop a simplified discrete element model with bonded spheres to model the ice cover. The breakage of ice cover can be obtained via the de-bonding process of bonded particles. Based on DEM simulations, the influence of ice velocity on ice load is obtained and compared with the experimental results. Moreover, the ice loads on upward and downward cones are also discussed.

2. DEM for interaction between ice cover and conical structure

A parallel bonding model is introduced to transfer the force and moment between bonded particles, as shown in Figure 1. Here, $\mathbf{X}^A$ and $\mathbf{X}^B$ are the position vectors of elements A and B, $\mathbf{F}_b^n$, $\mathbf{F}_b^s$ and $\mathbf{M}_b^n$, $\mathbf{M}_b^s$ are the normal and shear component vectors

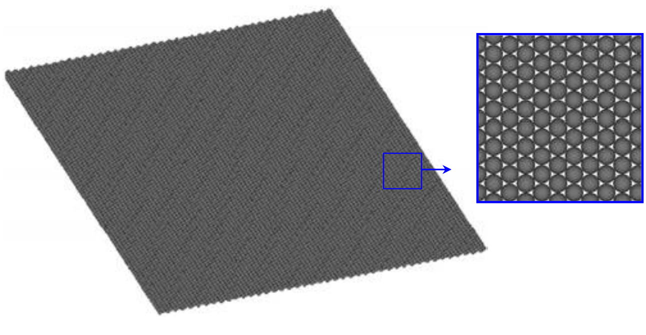

Figure 1.
Construction of level ice cover with bonded spherical particles

of force and moment, respectively. The parallel-bond glue is set over a circular cross section lying between the particles, and can transmit both force and moment (Potyondy and Cundall, 2004). The maximum normal and shear stresses within the bonding section are determined with the inter-particle force and moment. The total force and moment associated with the parallel bond are denoted by $\mathbf{F}_b$ and $\mathbf{M}_b$. Each of these vectors can be written into the normal and shear components as:

$$\mathbf{F}_b = \mathbf{F}_b^n + \mathbf{F}_b^s \tag{1}$$

$$\mathbf{M}_b = \mathbf{M}_b^n + \mathbf{M}_b^s \tag{2}$$

The maximum normal and tangential stresses in the bonding section can be determined as:

$$\sigma_{max} = \frac{|\mathbf{F}_b^n|}{A} + \frac{|\mathbf{M}_b^s|}{I} R \tag{3}$$

$$\tau_{max} = \frac{|\mathbf{F}_b^s|}{A} + \frac{|\mathbf{M}_b^n|}{J} R \tag{4}$$

where A, R, J and I are the area, radius, polar inertia moment and inertia moment of the bonding disk, respectively. Here we have $A = \pi R^2$, $J = \pi R^4/2$, $I = \pi R^4/4$, where R is the radius of bonding section.

For the sea ice materials, the brine volume is a key factor affecting its strength on a macro scale (Timco and Weeks, 2010; Ji *et al.*, 2011). The exponential function is introduced to link the flexural strength of sea ice and the brine volume. In this DEM simulation, the bonding strength has a similar relationship between inter-particle bonding strength and the brine volume on a micro scale. Here, we have:

$$\sigma_b = \beta(v_b)\sigma_b^{max} \quad \text{here } \beta = e^{-4.29\sqrt{v_b}} \tag{5}$$

where $\beta(v_b)$ is the reduction index of ice strength and is set as a function of brine volume, σ_b^{max} is the maximum bonding strength between ice particles.

The temperature and salinity can be combined as one parameter of brine volume with (Frankenstein and Garner, 1967):

$$v_b = S\left(0.532 + \frac{49.185}{|T|}\right) \tag{6}$$

where T is the ice temperature (°C), and S is the ice salinity(‰). Hence, the strength of sea ice under different temperatures and salinities can be determined.

The interaction between ice particles is calculated with an elastic-viscous contact model based on the Mohr-Coulomb shear friction law, as shown in Figure 2(b), where M_A and M_B are the mass of ice particle A and B, K_n and K_s are the normal and tangential stiffness, C_n and C_s are the normal and tangential damping coefficients, μ is the inter-particle friction coefficient.

Between two contacting ice particles, the normal force $\mathbf{F}_n = K_n\mathbf{x}_n - C_n\dot{\mathbf{x}}_n$ and the tangential force $\mathbf{F}_s = \min(|K_s\mathbf{x}_s - C_s\dot{\mathbf{x}}_s|, \mu|\mathbf{F}_n|) \cdot \mathbf{n}_s$. Here, $\mathbf{x}_n, \dot{\mathbf{x}}_n$ and $\mathbf{x}_s, \dot{\mathbf{x}}_s$ are the relative displacement and velocity of the two contacting particles in normal and tangential directions, respectively. $\mathbf{n}_s$ is the unit vector in tangential direction. Here, the

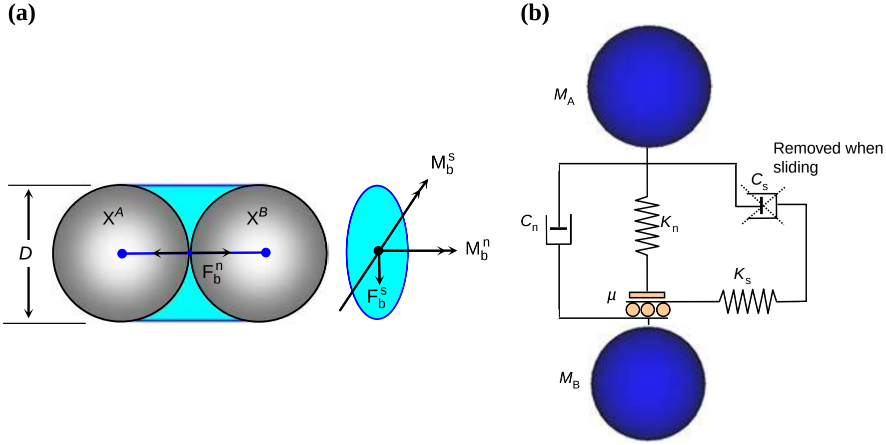

Figure 2. Parallel bonding model and contact force model of sea ice particles

Notes: (a) Parallel bonding model; (b) contact force model

damping coefficient $C_n = \zeta_n\sqrt{2MK_n}$, the dimensionless normal damping coefficient $\zeta_n = -\ln e/\sqrt{\pi^2+\ln^2 e}$, e is the coefficient of restitution. The normal and tangential stiffness have the relationship of $K_s = 0.5K_n$ and $C_s = 0.5C_n$ here.

3. Sensitive analysis of computational parameters on sea ice flexural strength

The flexural strength of sea ice is a key parameter in determining the ice load on conical offshore structure. A series of field and indoor physical tests have been carried out and the relationship between the sea ice flexural strength and sea ice parameters, such as ice temperature, salinity and sample size, has been obtained. Here, the influences of computational parameters in DEM simulations on sea ice flexural strength are analyzed under different element sizes, ice temperatures and salinities.

The sea ice sample size is designed as 70 mm high, 70 mm wide and 700 mm long. Here, we set the particle diameters (D) as 10, 15 and 20 mm, respectively, to study the influence of particle size on the flexural strength. The main computational parameters are listed in Table I. The bonding strength of sea ice is set the function of brine volume, which can be determined under given temperature and salinity by Equations (5) and (6).

The simulated bending failure processes are plotted as Figure 3 with different particle sizes. With different brine volumes, which are determined with various salinities and temperatures, the flexural strengths are determined with DEM simulated for different particle sizes. The fitted functions between ice brine volume and flexural strength are plotted in Figure 4 with different particle sizes. We can find the strength is independent of the particle size.

In the field experiments, the sea ice flexural strength was measured in different cold regions. Timco and Weeks (2010) found the flexural strength of sea ice has a negative exponential relationship to square root of brine volume. Ji *et al.* (2011) also determined the relationship between flexural strength and brine volume in the Bohai Sea. Both of their results are plotted in Figure 5. The results can be used to validate the DEM simulation data. We can find that the simulated result with regular packing is compared well with the experimental data. But the simulated data of irregular packing

Definition	Symbols	Values
Sample size	$b \times h \times L$	70 × 70 × 700 mm
Distance of loading points	L_0	500 mm
Particle size	D	10, 15, 20 mm
Particle-particle friction	μ_{pp}	0.1
Particle-particle restitution	e_{pp}	0.9
Loading rate	u	0.1 m/s
Elastic Modulus	E	10 MPa
Maximum bonding strength	σ_b^{max}	1.5 MPa
Ice salinity	S	0.1~7.0 ‰
Ice temperature	T	−20 ~ −1 °C
Brine volume	v_b	0.001 ~ 0.149

Table I. Computational parameters for DEM simulation of sea ice flexural strength

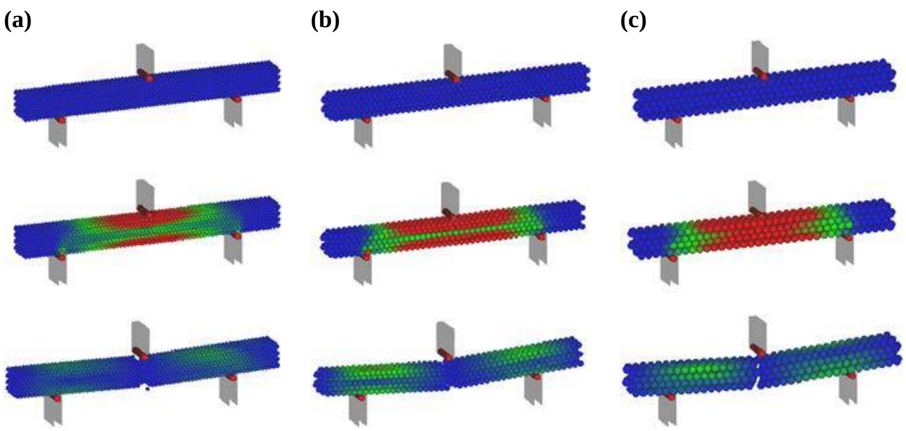

Notes: (a) D=10 mm; (b) D=15 mm; (c) D=20 mm

Figure 3. Bending failure process of sea ice simulated with DEM using different particle sizes

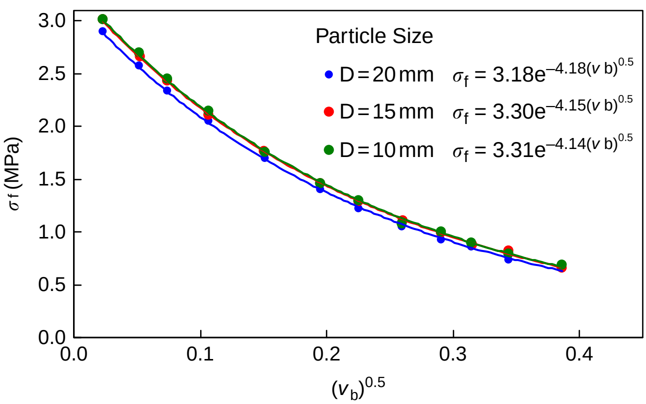

Figure 4. Comparison of sea ice flexural strengths under different particle sizes

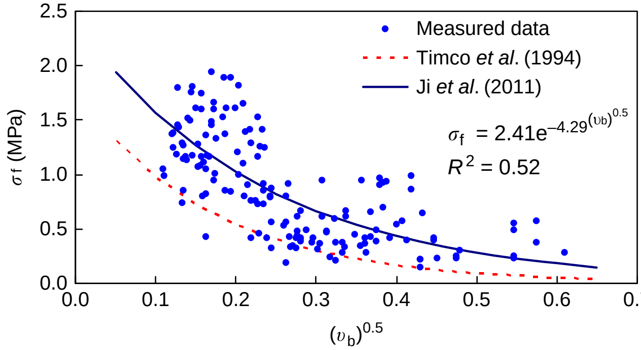

Figure 5.
Sea ice flexural strengths with physical experiments

is a little larger than the experimental data. It can be modified with adjusting the maximum bonding strength in the DEM simulation.

4. DEM simulation of ice load and compared with Hamburg Ship Model Basin (HSVA) experiment

4.1 HSVA experimental setup

The physical experiment of ice cover-conical structure interaction was performed in the ice tank of the HSVA in 2009. The ice tank is 78 m long by 10 m wide by 2.5 m deep. The model structure was mounted to a large towing carriage which can travel the length of the tank. Tests were conducted by moving the model structure at a determined speed through a stationary ice sheet. The model structure and its dimensions are shown in Figure 6. In this test, three different cones (narrow upward cone, wide upward cone and wide downward cone) were designed to investigate the influence of structure size and type on ice load. In this study, we simulate the ice load of narrow upward cone with the DEM under different ice velocities.

4.2 Simulation of ice loads on conical structure with DEM

In the DEM simulation of the interaction between ice cover and conical model structure performed in HSVA, the main computational parameters are listed in Table II. As the ice basin is too large for the DEM simulation, we only define a small square of ice sheet in front of the cone. This ice cover is larger than the diameter of cone to reduce the

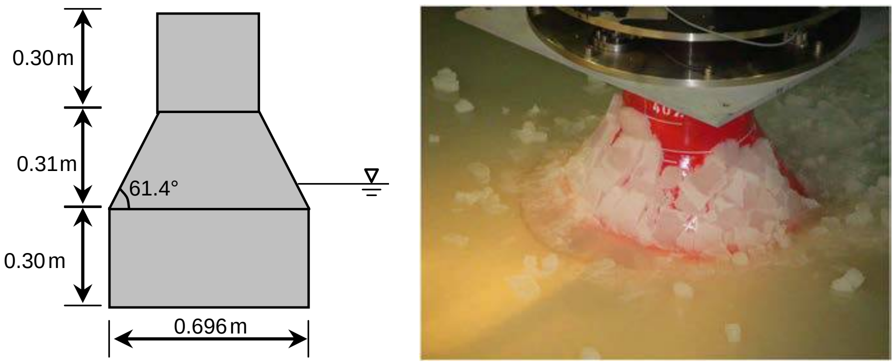

Figure 6.
The HSVA conical model structure for ice load tests

Definition	Symbol	Values
Sea ice density	ρ	920 kg/m^3
Ice cover size	$L \times b$	3.5 × 2.8 m
Ice thickness	H_{i}	0.032 m
Relative velocity	V_{i}	0.38 m/s
Normal stiffness of ice particle	K_{n}	2.6 × 10^7 N/m
Shear stiffness of ice particle	K_{s}	1.3 × 10^7 N/m
Particle-particle friction	μ_{pp}	0.1
Particle-particle restitution	e_{pp}	0.9
Wall-particle friction	μ_{wp}	0.1
Wall-particle restitution	e_{wp}	0.3
Maximum bonding strength	$\sigma_{\mathrm{b}}^{\max}$	0.5 MPa
Conical angle of model structure	θ	61.4°
Diameter of cone at water line	D	0.6 m
Model structure mass	M_{pile}	1.0 × 10^3 kg
Model structure damping ratio	ξ_{pile}	0.03
Model structure stiffness	K_{pile}	1.0 × 10^7 N/m

Table II. Main computational parameters in DEM simulation of interaction between ice cover and conical model structure in HSVA

boundary limitation. The particles at the left and right side boundaries of ice cover are fixed. The conical structure is dragged at a constant velocity. The model structure performs vibration under the collision of ice cover. The displacement and acceleration of model structure can also be determined when its mass, stiffness and damping ratio are defined.

With the DEM and its computational parameters above, the interaction between ice cover and conical model structure is simulated. The snapshots are shown in Figure 7 at different times. During the interaction between ice cover and model structure, the ice sheet breaks into small pieces when the inter-particle stress is larger than its bonding strength. The ice sheet breaks in both circumferential and radical failure modes in front of the ice-breaking cone. The phenomena have also been observed in the full-scale field observation in the Bohai Sea (Qu *et al.*, 2006; Wang *et al.*, 2012).

The simulated ice load in x direction is plotted in Figure 8(a), while the HSVA experimental data is plotted in Figure 8(b). From both of them, we can find the ice loads perform obvious impact characteristics. A dynamic ice load function and its spectrum

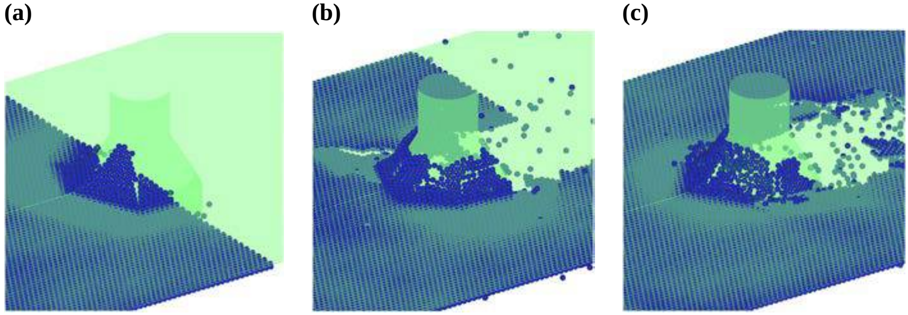

Notes: (a) t=1.7s; (b) t=4.5s; (c) t=7.0s

Figure 7. Snapshots of interaction between ice cover and ice-breaking cone under velocity $V_{\mathrm{i}} = 380$ mm/s

have been developed for conical structures based on field observations in the Bohai Sea (Qu *et al.*, 2006; Yue *et al.*, 2007). For a typical ice load function, the force period T, the ice force amplitude F_0, the ice climbing force F_c, and the ice bending failure force F_b are shown in Figure 9. The period and the maximum value of ice force are the key parameters in the ice load function, and are dominated with the velocity, thickness, strength of ice cover and the size and angle of the cone. The ice bending failure force plays a key role for the global ice force on ice-breaking cone. In the DEM simulation here, the maximum force $F_0 = 450$ N, the mean ice climbing force $F_c = 12.6$ N, and the ice bending failure force $F_b = 352.9$ N. In the HSVA experiment, we have $F_0 = 420$ N, $F_c = 25.5$ N, $F_b = 324.5$ N. The time-series of ice loads above are quite close in the DEM simulation and HSVA data. Therefore, the DEM simulation can catch the main characteristics of ice loads on conical structure.

4.3 Influence of relative velocity on ice load

To investigate the influence of velocity on ice load, five different drag velocities were performed in the HSVA tests as $V_i = 40, 100, 200, 380$ cm/s. The ice thickness $H_i = 32$ mm in all tests under different velocities. Here, we simulate the interaction of ice load on this conical model structure with different velocities with DEM. The experimental and simulated ice loads in x direction are plotted in Figure 10.

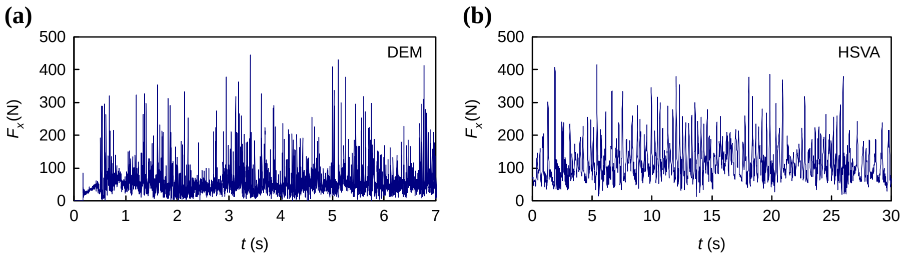

Notes: (a) DEM Simulation; (b) HSVA experiment

Figure 8. Ice load on ice-breaking cone in x direction under the relative velocity $V_i = 380$ mm/s

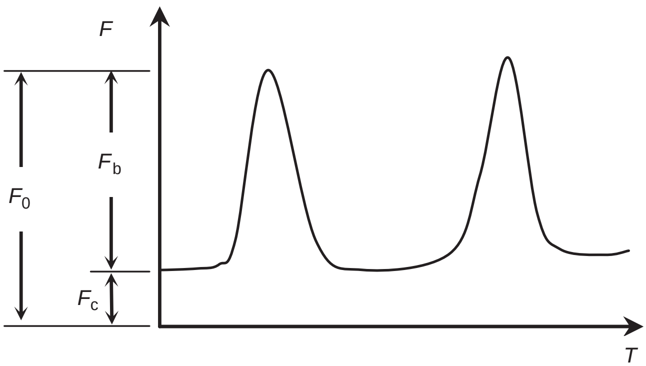

Notes: Here, T is the load period, F_0 is the ice load peak, F_c is the climbing ice load, F_b is the bending ice load

Figure 9. An ice load function on conical structure

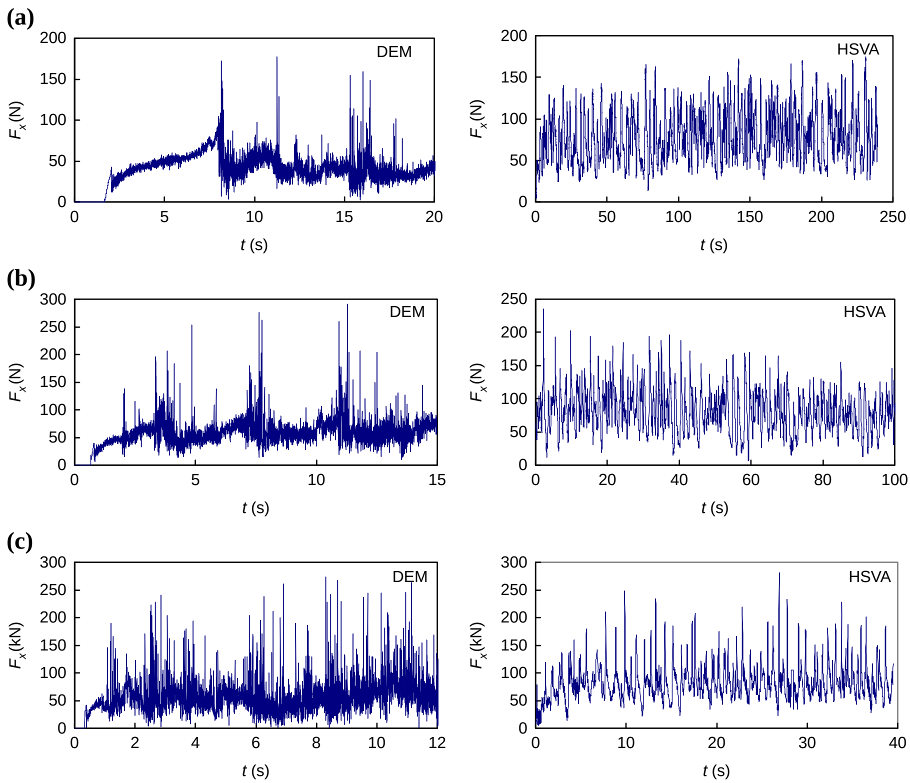

Notes: (a) Velocity $V_i = 40$ mm/s. Left is DEM results, and Right is HSVA data; (b) velocity $V_i = 100$ mm/s. Left is DEM results, and Right is HSVA data; (c) velocity $V_i = 200$ mm/s. Left is DEM results, and Right is HSVA data

Figure 10. Ice force in x direction obtained with DEM simulation and HSVA test

Because of the limitation of DEM computational efficiency, the dynamic duration of numerical simulation is much shorter than the HSVA data. To comprehensively compare the numerical data and experimental results, the maximum ice load, mean ice load and frequency of ice load are plotted in Figure 11. From both of them, we can find

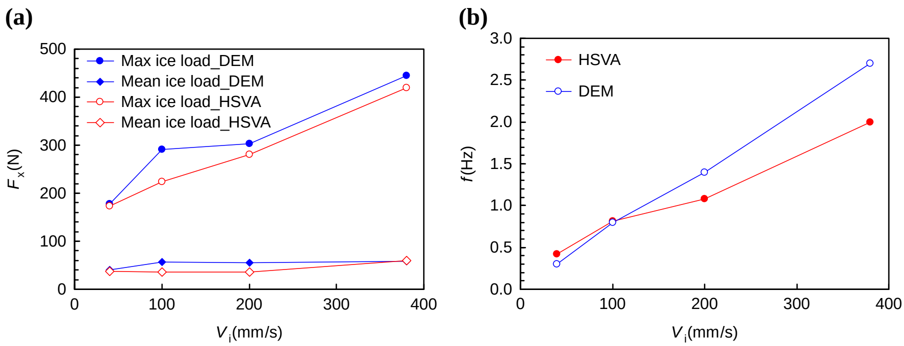

Notes: (a) Mean and maximum ice load; (b) frequency of ice load

Figure 11. Magnitude and frequency of ice loads under various ice velocities obtained with DEM simulation and HSVA test

the maximum value and frequency of ice load increase with increasing ice velocity. The DEM results compared well with that of the experimental data of HSVA.

5. Numerical simulation of ice load on upward-downward combined cone in the Bohai sea

5.1 Ice-breaking cone in the Bohai sea

In the Bohai Sea of China, about 20 conical jacket platforms were constructed in the last two decades. Most of them are combined with the top upward cone and the bottom downward cone. In this way, the cone height can be 4 m to cover the tidal height there. As the first conical jacket platform in the Bohai Sea, the JZ20-2 MNW and MUQ platforms are shown in Figure 12(a). The cone is combined by upward cone and downward cone, shown in Figure 12(b).

In DEM simulations of the interaction between sea ice and ice-breaking cone, the computational parameters are listed in Tables II and III. A square domain of ice cover is defined. The side boundaries are set moving with a constant ice velocity to drag the whole computational domain. The fixed conical pile can vibrate under the impact of ice cover.

(a) (b)

Figure 12. Conical jacket platforms in the Bohsai Sea

Notes: (a) JZ20-2 MNW and MUQ platforms; (b) ice-breaking cone

Table III. Main computational parameters of DEM simulation of dynamic ice load on conical structures

Definition	Symbol	Values
Ice cover size	$L \times b$	20×15 m
Ice thickness	t_i	0.2 m
Ice velocity	V_i	0.5 m/s
Particle normal stiffness	K_n	1.6×10^8 N/m
Particle shear stiffness	K_s	0.8×10^8 N/m
Sea ice salinity	S	6‰
Sea ice temperature	T	−10°C
Upward conical angle	θ_1	60°
Downward conical angle	θ_2	45°
Diameter of cone at water line	D	3.2 m
Mass of conical pile	M_{pile}	1.85×10^6 kg
Damping coefficient of conical pile	ξ_{pile}	0.03
Stiffness of conical pile	K_{pile}	2.0×10^8 N/m

5.2 Interaction between sea ice and upward and downward cones

For the upward cone, the snapshots simulated with DEM are plotted in Figure 13 at a different time. We can find the ice cover breaks into lots of pieces during the collision with the cone surface. The size of broken blocks is a key factor affecting the frequency and magnitude of ice load. Its probability distribution has been discussed in the field observation in the Bohai Sea (Yue *et al.*, 2007). The simulated ice loads in x and z directions are plotted in Figure 14. The maximum loads are 37.1 and 18.2 kN in x and z directions, respectively.

For the downward cone, the snapshots simulated with DEM are given in Figure 15, and the ice loads in x and z directions are plotted in Figure 16. The maximum ice loads are 18.1 and16.2 kN in x and z directions. We can find the ice load on downward cone is much lower than that on upward cone. The horizontal force on conical structure increases with increasing cone angle. Here, the angle of downward cone is 45°, which is much smaller than that of upward cone of 60°. The mechanism for the low ice load on downward cone will be analyzed in detail in a future study.

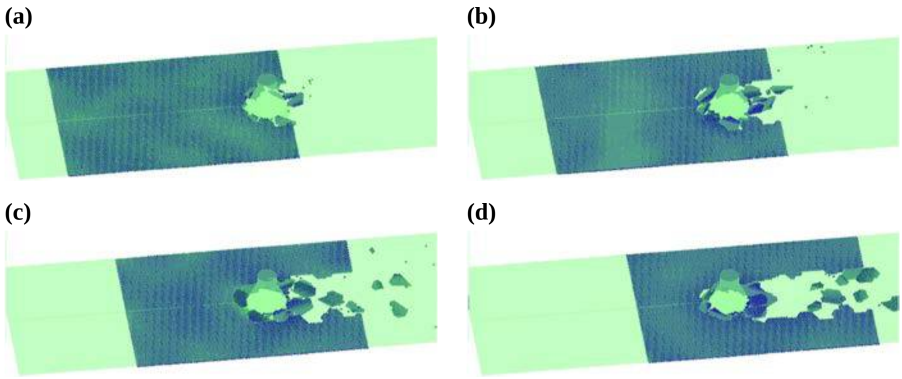

Notes: (a) t=12s; (b) t=20s; (c) t=36s; (d) t=55s

Figure 13. Snapshots of interaction between sea ice and upward cone simulated with DEM

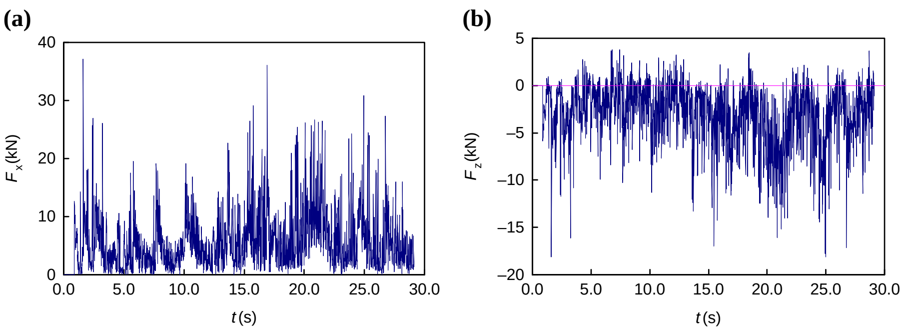

Notes: (a) Ice load in x direction; (b) ice load in z direction

Figure 14. Simulated dynamic ice load in x and z directions on upward ice-breaking cone

6. Conclusions

To determine the ice loads on conical offshore structure, the DEM is developed. The spherical particles are bonded to describe the ice cover. The interactions between ice cover and ice-breaking cone are simulated with DEM to determine the ice load. The influences of particle size, brine volume of sea ice on the flexural strength are discussed with DEM simulations. The simulated ice loads compared well with that measured in HSVA experiments under different velocities. The results show that the ice load increases with increasing ice velocity. Moreover, the ice loads on upward and downward cones are simulated with DEM using the cone size and shapes in the Bohai Sea. The ice load on downward cone is much lower than that on upward cone. The mechanism will be investigated with this DEM simulation in a future study.

DEM is an effective tool to study the ice load on offshore structures. In future studies, the computational parameters will be validated with the field data in the Bohai Sea. The ice-breaking length will be analyzed statistically with the DEM results. Moreover, the shielding effect on total ice load for multi-leg offshore structures and the CUDA-GPU computational technique for large computational scale will also be investigated.

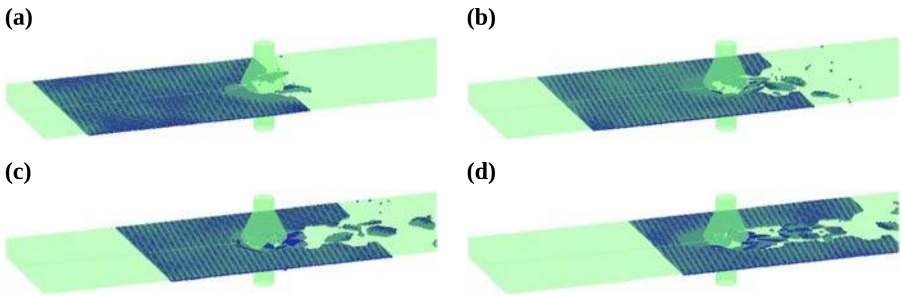

Notes: (a) t=10s; (b) t=24s; (c) t=38s; (d) t=55s

Figure 15. Snapshots of interaction between sea ice and downward cone simulated with DEM

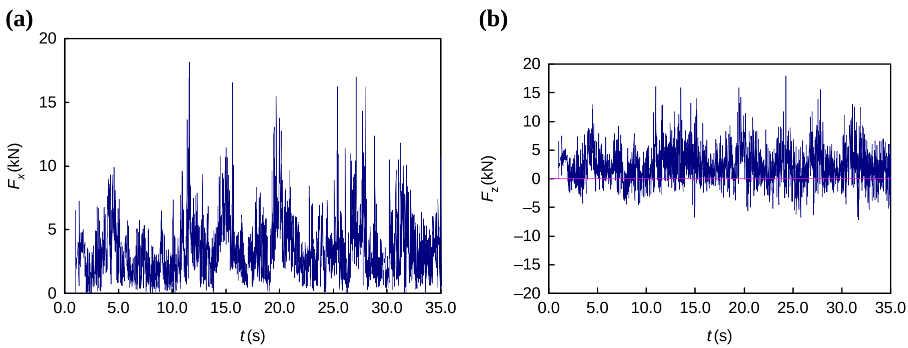

Notes: (a) Ice load in x direction; (b) ice load in z direction

Figure 16. Simulated dynamic ice load in x and z directions on downward ice-breaking cone

References

Brown, T.G. and Määttänen M. (2009), "Comparison of kemi-I and confederation bridge cone iceload measurement results", *Cold Regions Science and Technology*, Vol. 55, pp. 3-13.

Daley, C., Tuhkuri, J. and Riska, K. (1998), "The role of discrete failures in local ice loads", *Cold Regions Science and Technology*, Vol. 27, pp. 197-211.

Dempsey, J.P. (2000), "Research trends in ice mechanics", *International Journal of Solids and Structures*, Vol. 37, pp. 131-153.

Frankenstein, G. and Garner, R. (1967), "Equations for determining the brine volume sea ice from –0.5°C to –22.9°C", *Journal of Glaciology*, Vol. 6 No. 48, pp. 943-944.

Hansen, E.H. and Loset, S. (1999a), "Modelling floating offshore units moored in broken ice: model description", *Cold Regions Science and Technology*, Vol. 29, pp. 97-106.

Hansen, E.H. and Loset, S. (1999b), "Modelling floating offshore units moored in broken ice: comparing simulations with ice tank tests", *Cold Regions Science and Technology*, Vol. 29, pp. 107-119.

Hopkins, M.A., Frankenstein, S. and Thorndike, A.S. (2004), "Formation of an aggregate scale in Arctic sea ice", *Journal of Geophysical Research*, Vol. 109 No. C11, pp. 1-10.

Huang, Y. and Li, X. (2011), "Dynamic ice loads on conical structures", *Theoretical & Applied Mechanics Letters*, Vol. 1 No. 022007, pp. 1-3.

Ji, S., Wang, A., Su J. and Yue, Q. (2011), "Experimental studies on elastic modulus and flexural strength of sea ice in the Bohai sea", *ASCE Journal of Cold Regions Engineering*, Vol. 25 No. 4, pp. 182-195.

Lau, M., Lawrence, K.P. and Rothenburg, L. (2011), "Discrete element analysis of ice loads on ships and structures", *Ships and Offshore Structures*, Vol. 6 No. 3, pp. 211-221.

Paavilainen, J. and Tuhkuri, J. (2012), "Parameter effects on simulated ice rubbling forces on a wide sloping structure", *Cold Regions Science and Technology*, Vol. 81, pp. 1-10.

Polojarvi, A., Tuhkuri, J. and Korkalo, O. (2012), "Comparison and analysis of experimental and virtual laboratory scale punch through tests", *Cold Regions Science and Technology*, Vol. 81, pp. 11-25.

Potyondy, D.O. and Cundall, P.A. (2004), "A bonded-particle model for rock", *International Journal of Rock Mechanics & Mining Sciences*, Vol. 41, pp. 1329-1364.

Qu, Y., Yue, Q., Bi, X. and Kärnä, T. (2006), "A random ice force model for narrow conical structures", *Cold Regions Science and Technology*, Vol. 45, pp. 148-157.

Selvadurai, A.P.S. and Sepehr, K. (1999), "Two-dimensional discrete element simulations of ice-structure interaction", *Interactional Journal of Solids and Structures*, Vol. 36, pp. 4919-4940.

Sun, S. and Shen, H.H. (2011), "Simulation of pancake ice load on a circular cylinder in a wave and current field", *Cold Regions Science and Technology*, Vol. 78, pp. 31-39.

Timco, G.W. and Weeks, W.F. (2010), "A review of engineering properties of sea ice", *Cold Regions Science and Technology*, Vol. 60, pp. 107-129.

Wang, Y., Yue, Q., Guo, F., Bi, X., Shi, Z. and Qu, Y. (2012), "Performance evaluation of a new ice-resistant jacket platform based on field monitoring", *Cold Regions Science and Technology*, Vol. 71, pp. 44-53.

Yue, Q. and Bi, X. (2000), "Ice induced jacket structure vibration", *Journal of Cold Regions Engineering*, Vol. 14 No. 2, pp. 81-92.

Yue, Q., Qu, Y., Bi, X. and Karna, T. (2007), "Ice force spectrum on narrow conical structures", *Cold Regions Science and Technology*, Vol. 49, pp. 161-169.

Further reading

Arenson, L.U. (2004), "Numerically modelling the strength of ice using discrete elements", *Proceedings of the 2nd PFC Symposium, Kyoto, October 28-29*.

Frederking, R. and Sudom, D. (2006), "Maximum ice force on the Molikpaq during the April 12, 1986 event", *Cold Regions Science and Technology*, Vol. 46, pp. 147–166.

Hopkins, M.A. (1996), "On the mesosacle interaction of lead ice and floes", *Journal of Geophysical Research*, Vol. 101 No. C8, pp. 18315-18326.

Hopkins, M.A. (1997), "Onshore ice pile-up: a comparison between experiments and simulations", *Cold Regions Science and Technology* Vol. 26 No. 3, pp. 205-214.

Huang, Y. (2010), "Model test study of the nonsimultaneous failure of ice before wide conical structures", *Cold Regions Science and Technology*, Vol. 63, pp. 87-96.

Kioka, S., Yamamoto, Y., Mori, M. and Takeuchi, T. (2009), "Medium-scale test and numerical simulation using DEM for the impact load by a high speed ice floe against a structure", *Proceedings of the 20th International Conference on Port and Ocean Engineering under Arctic Conditions POAC09-36, Luleå, June 9-12, 2009*.

Xu, N., Yue, Q.J., Qu, Y. and Bi, X.J. and Palmer, A. (2011), "Results of field monitoring on ice actions on conical structures", *Journal of Ocean Mechanics and Engineering*, Vol. 133, p. 041502.

Corresponding author
Professor Shunying Ji can be contacted at: jisy@dlut.edu.cn